Title

Accurate Classical Polarization Solution with No Self-Consistent Field Iterations

Journal

The Journal of Physical Chemistry Letters, 8(8)

ISSN

1948-7185

Authors

Albaugh, Alex

Niklasson, Anders MN

Head-Gordon, Teresa

Publication Date

2017-04-20

DOI

10.1021/acs.jpclett.7b00450

Peer reviewed

Accurate Classical Polarization Solution with No Self-Consistent Field Iterations

Alex Albaugh[1], Anders M. N Niklasson[4], and Teresa Head-Gordon[1,2,3,5*]

Departments of [1]Chemical and Biomolecular Engineering, [2]Chemistry, and [3]Bioengineering, University of California, Berkeley, CA 94720

[4]Theoretical Division, Los Alamos National Laboratory, Los Alamos, NM 87545

[5]Chemical Sciences Division, Lawrence Berkeley National Laboratory, University of California, Berkeley, CA 94720

We present a new solution for classical polarization that does not require any self-consistent field iterations, the aspect of classical polarization that makes it computationally expensive. The new method builds upon our iEL/SCF Lagrangian scheme that defines a set of auxiliary induced dipoles whose original purpose was to serve as a time-reversible initial guess to the SCF solution of the set of real induced dipoles. In the new iEL/0-SCF approach the auxiliary dipoles now drive the time evolution of the real induced dipoles such that they stay close to the Born-Oppenheimer surface in order to achieve a truly SCF-less method. We show the iEL/0-SCF exhibits no loss of simulation accuracy when analyzed across bulk water, low to high concentration salt solutions, and small solutes to large proteins in water. In addition, iEL/0-SCF offers significant computational savings over more expensive SCF calculations based on traditional 1 fs time step integration using symplectic integrators and is as fast as reversible reference system propagator algorithms with an outer 2 fs time step.

TOC Graphic

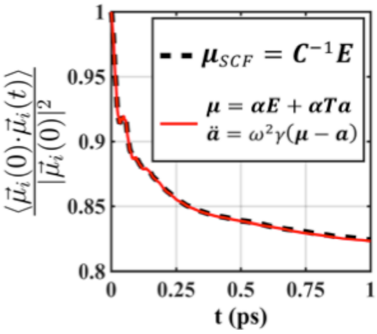

*Corresponding author:
Stanley 274
510-666-2744 (V)
thg@berkeley.edu

INTRODUCTION

Polarization, the ability of a molecule's electron density to deform, respond, and influence its environment, is the leading order many-body interaction for advanced electrostatics used in molecular simulation.[1-4] It has proven to be an important interaction that accurately captures intermolecular interactions of ligand bound complexes[5], heterogeneity at interfaces[6-7], electric field environments of heterogeneous systems such as proteins[8-9], structure and dynamics of peptide-water solutions[10-11], and it also has been shown to be more transferable across the phase diagram of liquid water beyond the regions where the force field was initially parameterized[12].

Complete convergence of mutual polarization is usually solved using an iterative self-consistent field method (SCF) to determine a set of induced electrical dipoles within the system[13-14]. Self-consistent iteration is usually preferred over dynamic methods such as extended Lagrangians (EL)[15-16] because of the better stability with larger time steps. However, the repeated iteration can be a significant computational cost even with the adoption of advanced SCF solvers such as the preconditioned conjugated gradient (PCG)[13] or direct inversion of the iterative subspace (DIIS)[14, 17-18] methods. Recently, several novel methods have been introduced with the aim of achieving better energy conservation and/or reducing the number of SCF iterations, without sacrificing accuracy. The classical iAMOEBA[12] approach chooses to only account for direct polarization, i.e. the response of inducible dipoles to the permanent electrostatics with no mutual induction, thereby completely avoiding the iterative SCF step altogether. The extrapolated perturbation theory (ExPT) is a method that uses a perturbation series for the polarization energy which is truncated at low order and then extrapolated to infinite order to recover an approximation of the true, fully converged SCF solution[19]. In both of these cases there are some sacrifices to polarization accuracy that must be recovered through either reparameterization of the underlying force field as done for iAMOEBA or parameter adjustments of the method in the case of ExPT[20] that have led to significant improvements through the OPTn methods[21]. While recent approaches such as OPT4[19] and the truncated conjugate gradient TCG[22] have improved polarization solution accuracy compared to ExPT, they have not been able to fully eliminate the cost of polarization, i.e. to eliminate the need to perform any SCF iterations.

Another approach due to Niklasson and colleagues[23-27] starts from the broken time-reversal symmetry problem in Born Oppenheimer molecular dynamics (BOMD) to derive a time-reversible extrapolation scheme for the electronic degrees of freedom. Equivalently, it can be formulated in the form of an extended Lagrangian in which an additional set of auxiliary electronic degrees of freedom are propagated alongside the nuclei with the purpose of generating either good quality time-reversal guesses for the SCF calculations, or as a stand-alone SCF-free extended Lagrangian formulation of BOMD. Albaugh *et al.* extended the time-reversible extrapolation scheme to the solution for classical polarization

using an extended Lagrangian solution for an auxiliary set of induced dipoles that serve as an initial guess for the SCF solution of real dipoles[28]. It is known that the numerical error in the SCF solutions (which are never exact due to incomplete convergence and/or an approximate numerical algebra) will leak back to the auxiliary degrees of freedom and give rise to instabilities in their equations of motion[26, 28-29]. To address this problem Niklasson and co-workers have proposed a dissipative integration scheme for the equations of motion of the electronic degrees of freedom using a modified form of the Verlet algorithm that controls the numerical instability at the expense of a small amount of broken time-reversibility[26]. By contrast, Albaugh *et al.* chose to couple the auxiliary velocities to a thermostat to prevent buildup of inertia, thus preserving time-reversibility (which we refer to as an inertial extended Lagrangian, iEL/SCF), through the use of a time-reversible solution to Nosé-Hoover thermostat variables for the auxiliary degrees of freedom[28].

While we have shown that the iEL/SCF methods reduces the number of SCF iterations required by half for classical polarization[28], and much more for linear scaling density functional theory (DFT) in the BOMD code of ONETEP[29], it did not eliminate the need for SCF iterations completely. In this work we introduce an extension of the iEL/SCF method that eliminates the SCF step altogether in classical molecular dynamics simulations with polarizable induced dipoles, which we refer to as the iEL/0-SCF method. The iEL/0-SCF scheme presented here is not a straightforward extension of the SCF-less XL-BOMD scheme[27] to polarizable force fields, but differs in significant ways as we show below. We find that the iEL/0-SCF approach is as accurate as standard SCF approaches for pure water, dilute to concentrated salt solutions, and small peptides and large proteins in water. In the TINKER implementation of the iEL/0-SCF approach we show that it also scales better under OpenMP parallelization than the standard SCF solvers, such that it is faster and at least as accurate as the default SCF scheme using either Verlet or a simple multi-time step technique such as the reversible reference system propagator algorithms (RESPA)[30] that uses a 2.0 fs outer time step. In summary, the iEL/0-SCF approach offers a complete and accurate mutual polarization solution at the cost of direct polarization.

THEORY

To achieve a polarization scheme that does not require SCF iterations, we start with a Lagrangian for a classical system of *N* atoms and examine how self-consistently iterated induced dipoles on each atom contribute to the potential:

$$\mathcal{L}(\boldsymbol{r^N}, \dot{\boldsymbol{r}}^{\boldsymbol{N}}) = \frac{1}{2}\sum_{i=1}^{N} m_i \dot{\boldsymbol{r}}_i^2 - U(\boldsymbol{r^N}, \boldsymbol{\mu}^N) \quad (1)$$

In Eq. (1) $\boldsymbol{r}_i$ and $\dot{\boldsymbol{r}}_i$ are the position and velocity of the *i*-th atom, respectively, and $U(\boldsymbol{r^N}, \boldsymbol{\mu}^N)$ is the potential energy for the current atomic configuration. Here the potential energy can be broken into both a

many-body polarization energy contribution, $U^{polar}\left(\boldsymbol{r^N}, \boldsymbol{\mu}_{SCF}^{N}\right)$, and all other contributions, $U^{other}(\boldsymbol{r^N})$, which can include non-bonded terms such as permanent electrostatic and van der Waals interactions and bonded valence terms like bond-stretching, angle-bending, torsionals, and others.

$$U(\boldsymbol{r^N}, \boldsymbol{\mu}^N) = U^{other}(\boldsymbol{r^N}) + U^{polar}(\boldsymbol{r^N}, \boldsymbol{\mu}^N) \tag{2}$$

Assuming complete convergence of the induced dipoles to their SCF solutions, $\boldsymbol{\mu_{SCF}}$, the component of the potential energy that depends on polarization, $U^{polar}(\boldsymbol{r^N}, \boldsymbol{\mu}^N)$, can be given as

$$U_{SCF}^{polar}\left(\boldsymbol{r^N}, \boldsymbol{\mu}_{SCF}^{N}\right) = -\frac{1}{2}\boldsymbol{\mu}_{SCF}^{T}\boldsymbol{E} \tag{3}$$

and where

$$\boldsymbol{\mu_{SCF,i}} = \alpha_i \boldsymbol{E}_i + \alpha_i \sum_{j=1}^{N} \boldsymbol{T}'_{ij}\boldsymbol{\mu_{SCF,j}}; \tag{4}$$

Here $\boldsymbol{E}_i$ is the electric field contribution at site *i* due to permanent electrostatics in the system (fixed charges, dipoles, quadrupoles, etc.), $\boldsymbol{T}'_{ij}$ is the induced dipole interaction matrix between sites *i* and *j*, and α_i, is the atomic polarizability of the *i*-th atom. We can cast Eq. (4) in terms of a super-matrix $\boldsymbol{C}$

$$\boldsymbol{\mu_{SCF}} = \boldsymbol{C^{-1}E} \tag{5}$$

whose blocks are given by $\boldsymbol{C}_{ij} = (\alpha_j^{-1}\delta_{ij} - \boldsymbol{T}'_{ij})$. While the induced dipoles can be solved exactly through matrix inversion, as is done for two and three-body polarization interactions in our recent 3m-AMOEBA model[31], in practice it is prohibitively expensive to perform this calculation for very large systems as it involves inverting the 3*N* by 3*N* $\boldsymbol{C}$ super matrix.

Usually Eq. (5) is solved iteratively using standard SCF methods such as PCG due to Wang and Skeel[13] to some tolerance, usually with a predictor to accelerate the convergence of the SCF problem. However, predictors that use information from previous steps break time reversibility in the context of molecular dynamics, leading to an inevitable degradation in energy conservation. An alternative to solving for the many-body electronic problem that avoids a self-consistent solution was originally addressed by Car and Parrinello[32]. In their seminal work they formulate an extended Lagrangian (EL) to evolve the electronic degrees of freedom dynamically by introducing fictitious masses, and the EL approach was extended to induced dipole polarization by Wodak and co-workers[16]. Overall, standard EL solutions to both quantum[32] and classical[15, 33] electronic degrees of freedom are found to be stable and conserve energy, but only for reduced and sometimes very small time steps that precludes their practical use in molecular simulation[28] unless significant numerical error is tolerated.

Niklasson *et al.* tackled the problem of broken time-reversibility of the electronic dynamics through a distinct formalism[23] that can also be expressed in a Lagrangian formulation[26-27], which Albaugh and co-workers have recently adapted for classical polarization[28] as shown in Eq. (6)

$$\mathcal{L}'^{(\boldsymbol{r}^N,\dot{\boldsymbol{r}}^N,\boldsymbol{a}^N,\dot{\boldsymbol{a}}^N)} = \frac{1}{2}\sum_{i=1}^{N} m_i \dot{\boldsymbol{r}}_i^2 + \frac{1}{2}\sum_{i=1}^{N} m_{a,i}\, \dot{\boldsymbol{a}}_i^2 - U(\boldsymbol{r}^N, \boldsymbol{a}^N) - \frac{1}{2}\omega^2 \sum_{i=1}^{N} m_{a,i} \left(\boldsymbol{\mu}_{SCF,i} - \boldsymbol{a}_i\right)^2 \quad (6)$$

Here $\boldsymbol{a}_i$ and $\dot{\boldsymbol{a}}_i$ are the auxiliary induced dipole and corresponding velocity for atom i, each of which has a fictitious mass associated with it, $m_{a,i}$. The additional terms in the Lagrangian are now a kinetic energy associated with the auxiliary dipoles and a harmonic potential that aims to keep the auxiliary dipoles close to the true SCF dipoles, which in turn is determined by the steepness of this harmonic well and characterized by a frequency ω. It has been shown that for a time-reversible Verlet integration algorithm with a finite integration time step Δt, the maximum stable value of ω is $\sqrt{2}/\Delta t$.[27] These auxiliary variables then serve as good initial guesses to the SCF solution for the real dipoles to reach the final solution, $\boldsymbol{\mu}_{SCF,i}$ and with notable improvements in energy conservation[25, 28]. However, in practice the iterative solution of the induced dipoles never reaches the exact solution, as the iteration is stopped at some convergence threshold. This error couples to the auxiliary degrees of freedom through the potential (last term in Eq. (6)), which corrupts the auxiliary dynamics such that they become more and more poor initial guesses for the real degrees of freedom, and the number of SCF cycles increases without bound[28].

Niklasson proposed the introduction of dissipation for this numerical error that achieves only a small amount of broken time-reversibility since it is introduced at an order commensurate with the integration error.[26] Unfortunately when the dissipative force is combined with the accurate classical polarization force, the dissipation scheme unambiguously exhibits energy drift. An alternative approach taken by Albaugh and co-workers was to introduce a simple thermostating scheme, illustrated using both Berendsen weak coupling and Nosé-Hoover chain thermostats, applied to the auxiliary dipole velocities.[28] The latter case, i.e. the inertial iEL/SCF method, was shown to provide superior energy conservation with less stringent convergence thresholds and a correspondingly small number of SCF cycles, to reproduce all properties of the classical polarization model in the NVT and NVE ensembles accurately.

Now turning to the problem of achieving an iteration-free dynamics for the electronic degrees of freedom, given this background, we introduce modifications to the Lagrangian in Eq. (6) in two important ways. First we introduce a general form for the polarization potential energy that does not assume convergence of the real induced dipoles[20]

$$U^{polar}(\boldsymbol{r}^N, \boldsymbol{a}^N) = \frac{1}{2}\boldsymbol{\mu}^T \boldsymbol{C}\boldsymbol{\mu} - \boldsymbol{\mu}^T \boldsymbol{E} \quad (7)$$

This means that if the real dipole differs from the exact self-consistent solution by a small amount $\boldsymbol{\delta}$, $\boldsymbol{\mu} = \boldsymbol{\mu}_{SCF} + \boldsymbol{\delta}$, the polarization potential differs from the exact self-consistent solution by an order of the square of the error, $\boldsymbol{\delta}^2$. To see this one can substitute $\boldsymbol{\mu} = \boldsymbol{\mu}_{SCF} + \boldsymbol{\delta}$ into Eq. (7),

$$U^{polar} = \frac{1}{2}(\boldsymbol{\mu}_{SCF} + \boldsymbol{\delta})^T \boldsymbol{C}(\boldsymbol{\mu}_{SCF} + \boldsymbol{\delta}) - (\boldsymbol{\mu}_{SCF} + \boldsymbol{\delta})^T \boldsymbol{E} = -\frac{1}{2}\boldsymbol{\mu}_{SCF}{}^T \boldsymbol{E} + \frac{1}{2}\boldsymbol{\delta}^T \boldsymbol{C}\boldsymbol{\delta} \quad (8)$$

which makes use of the requirement that for completely converged induced dipoles $\boldsymbol{C\mu_{SCF}} - \boldsymbol{E} = \boldsymbol{0}$. The difference between the general potential and the exact solution is

$$U^{polar} - U_{SCF}^{polar} = \frac{1}{2}\boldsymbol{\delta^T C \delta} = O(|\boldsymbol{\delta}|^2) \tag{9}$$

so that for any small errors in the induced dipoles that result from no iteration, we push the error in the potential to second order. The same analysis applies to the gradient of this potential, which affects the forces for dynamics and is what is relevant in molecular dynamics. After differentiating Eq. (8)

$$\frac{dU^{polar}}{d\boldsymbol{r}} = \frac{1}{2}\boldsymbol{\mu_{SCF}}^T \frac{\partial \boldsymbol{C}}{\partial \boldsymbol{r}} \boldsymbol{\mu_{SCF}} - \boldsymbol{\mu_{SCF}}^T \frac{\partial \boldsymbol{E}}{\partial \boldsymbol{r}} + \frac{1}{2}\boldsymbol{\delta^T} \frac{\partial \boldsymbol{C}}{\partial \boldsymbol{r}} \boldsymbol{\delta} \tag{10}$$

and recognizing that

$$\frac{dU_{SCF}^{polar}}{d\boldsymbol{r}} = \frac{1}{2}\boldsymbol{\mu_{SCF}}^T \frac{\partial \boldsymbol{C}}{\partial \boldsymbol{r}} \boldsymbol{\mu_{SCF}} - \boldsymbol{\mu_{SCF}}^T \frac{\partial \boldsymbol{E}}{\partial \boldsymbol{r}} \tag{11a}$$

and

$$\left(\frac{\partial \boldsymbol{C}}{\partial \boldsymbol{r}} \boldsymbol{\mu_{SCF}} + \boldsymbol{C} \frac{\partial \boldsymbol{\mu_{SCF}}}{\partial \boldsymbol{r}} - \frac{\partial \boldsymbol{E}}{\partial \boldsymbol{r}}\right) = \boldsymbol{0} \tag{11b}$$

we again confirm that error in the forces are also second order

$$\frac{dU^{polar}}{d\boldsymbol{r}} - \frac{dU_{SCF}^{polar}}{d\boldsymbol{r}} = \frac{1}{2}\boldsymbol{\delta^T} \frac{\partial \boldsymbol{C}}{\partial \boldsymbol{r}} \boldsymbol{\delta} = O(|\boldsymbol{\delta}|^2) \tag{12}$$

The second important ingredient is to control the error quantity $\boldsymbol{\delta}$. Like the iEL/SCF procedure, the real induced dipoles will depend explicitly on using the auxiliary dipoles as an initial guess

$$\boldsymbol{\mu_i} = \alpha_i \boldsymbol{E}_i + \alpha_i \sum_{j=1}^{N} \boldsymbol{T'_{ij}} \boldsymbol{a}_j \tag{13}$$

but in this case we perform no SCF cycles. Instead we define $\boldsymbol{\mu}_{SCF,i}$ from simple linear mixing of the real and auxiliary induced dipoles via a local kernel approximation[27]

$$\boldsymbol{\mu}_{SCF,i} \approx \gamma \boldsymbol{\mu}_i + (1 - \gamma)\boldsymbol{a}_i \tag{14}$$

where γ is an adjustable mixing parameter that will need to be tuned. This is similar in spirit to a predictor-corrector scheme[34] in which Eq. (13) gives a prediction of the converged induced dipoles from the auxiliary dipoles, and then Eq. (14) serves as a correction by mixing the time reversible solution corresponding to the auxiliary variables with the solution for the real dipoles. While more complicated forms of approximating the SCF dipole are possible, such as a non-local kernel method[27], we find that this simple approximation works well for all cases shown in the Results. To be clear Eq. (14) is not used for the calculation of the true polarization energy and forces, but only applies to the derivation of the auxiliary equation of motion as we show below. It is now clear that the real dipoles, $\boldsymbol{\mu}$, are dependent on the auxiliary dipoles, $\boldsymbol{a}$, so that the potential in Eq. (6) is now dependent on position and auxiliary dipoles, $U(\boldsymbol{r^N}, \boldsymbol{a^N})$ instead of $U(\boldsymbol{r^N}, \boldsymbol{\mu^N})$ previously in Eq. (1).

We now apply the Euler-Lagrange equation to the Lagrangian in Eq. (6) for both the real coordinates $\boldsymbol{r^N}$ and the auxiliary dipoles $\boldsymbol{a^N}$ to obtain equations of motion for each

$$m_i\ddot{\boldsymbol{r}}_i = -\frac{dU(\boldsymbol{r^N},\boldsymbol{a^N})}{d\boldsymbol{r}_i}\Big|_{\boldsymbol{a^N}} \tag{15}$$

$$m_{a,i}\ddot{\boldsymbol{\alpha}}_i = \omega^2 m_{a,i}\left(\boldsymbol{\mu}_{SCF,i} - \boldsymbol{a}_i\right) + \sum_{j=1}^{N}\left(\alpha_j^{-1}\delta_{ij} - \boldsymbol{T}'_{ij}\right)(\boldsymbol{\mu}_j - \boldsymbol{a}_j) \tag{16}$$

Eq. (15) is the familiar statement of Newton's law for the nuclei where the gradients of the various forms of the potential energy on the right hand side remain in their usual forms, except for the polarization potential energy, which now depends on the auxiliary dipoles directly as seen in form of Eq. (7). Eq. (16) gives the equation of motion for the auxiliary dipoles, which we note has an extra term proportional to $(\boldsymbol{\mu} - \boldsymbol{a})$; it can be formally shown that by assuming $m_a \sim 1/\omega^2$, and in the limit that $m_{a,i} \to 0$ and $\omega \to \infty$ such that $\omega m_{a,i} =$ constant, we recover an adiabatic Born-Oppenheimer-like approximation of the auxiliary dipole moment. In practice we will show *a posteriori* that indeed this term is negligible and can (and will be) ignored. When Eq. (14) is substituted into the auxiliary equation of motion in Eq. (16), we obtain the final form

$$\ddot{\boldsymbol{\alpha}}_i = \omega^2\gamma(\boldsymbol{\mu}_i - \boldsymbol{a}_i) \tag{17}$$

Of course for dynamics we will also need the forms of the gradient to calculate forces. In this case we use the complete polarization gradient

$$\frac{dU^{pol}(\boldsymbol{r^N})}{d\boldsymbol{r}} = \frac{\partial U^{pol}(\boldsymbol{r^N})}{\partial \boldsymbol{r}} + \frac{\partial U^{pol}(\boldsymbol{r^N})}{\partial \boldsymbol{\mu}}\frac{\partial \boldsymbol{\mu}}{\partial \boldsymbol{r}} \tag{18}$$

The first term on the right hand side of Eq. (18) is the nuclear term and the second term is the dipole response term, which goes to 0 in the limit of perfectly converged induced dipoles[19-20]. In practice, although perfect convergence can never be achieved, the dipole response term is typically not explicitly calculated with the understanding that this is a good approximation for a tight level of SCF convergence. With the iEL/0-SCF approach, however, we need the dipole response term, since our analytical polarization potential requires it, unlike the iterative SCF solvers. Since we have an explicit position dependence of our dipoles, defined by Eq. (13), it is straightforward to calculate these dipole response terms with no additional algorithmic expense. Substituting Eq. (7) and (13) into Eq. (18) we obtain the final form of the gradient used for dynamics

$$\frac{dU^{pol}(\boldsymbol{r^N})}{d\boldsymbol{r}} = -\frac{1}{2}\boldsymbol{\mu}^T\frac{\partial \boldsymbol{T'}}{\partial \boldsymbol{r}}\boldsymbol{\mu} - \left[(\alpha \boldsymbol{T}\boldsymbol{\mu})^T + (\alpha \boldsymbol{E})^T - \boldsymbol{\mu}^T\right]\frac{\partial \boldsymbol{T'}}{\partial \boldsymbol{r}}\boldsymbol{a} - \left[(\alpha \boldsymbol{T}\boldsymbol{\mu})^T + (\alpha \boldsymbol{E})^T\right]\frac{\partial \boldsymbol{TM}}{\partial \boldsymbol{r}} \tag{19}$$

Finally, the AMOEBA potential has additional features of electrostatic and polarization scaling that are further discussed in Appendix A, knowledge required to reproduce the results shown later in Results.

METHODS

The modifications to the polarization potential and gradient and the addition of auxiliary induced dipoles were introduced into the TINKER software package[35]. For pure water systems we used the AMOEBA14 force field[36] which used Force Balance[37] to optimize the AMOEBA parameters for better description of water properties. For other systems, such as three concentrations of magnesium chloride salt solutions and the solvated dihydrofolate reductase (DHFR) protein, we used the AMOEBABIO09[38] force field, a general purpose biomolecular parameterization of the Amoeba functional form. For the solvated zwitterionic glycine peptide ($+NH_3$-C_αH-COO–), we use the AMOEBA parameters derived from recent work comparing its decomposed THz spectra with *ab initio* molecular dynamics.[39] Further details of the simulation protocol are described in the SI material.

The primary difference investigated in this work is how mutual polarization is treated. The iEL/0-SCF simulations were initiated with real and auxiliary dipoles that were solved to a very tightly converged solution of 10^{-9} RMS Debye. A velocity Verlet integration scheme[40] was then used to propagate the auxiliary induced dipoles and dipole velocities with a 0.5 fs time step in the NVE ensemble and with a 1.0 fs time step in the NVT ensemble. To determine an optimal γ for a given system, short (~100 ps) NVE trajectories were run over the range of possible γ values (0 to 1.0) and the γ of the trajectory with the lowest energy drift was selected for production.

For the NVT ensemble, auxiliary dipoles were thermostated using a 4th-order Nosé-Hoover chain[41] as described in previous work[28]; the set point of the auxiliary dipole pseudo-temperature was 5.3 $e^2Å^2/ps^2$, which we found to be the natural temperature of well-integrated, stable iEL/0-SCF simulations at small time steps. For comparison purposes, simulations performed with a standard preconditioned conjugate gradient SCF (PCG-SCF)[13] iterative procedure were calculated using an SCF convergence threshold of 10^{-6} RMS Debye, which is an order of magnitude tighter than the TINKER default in order to absolutely ensure accurate data for comparison purposes.

RESULTS

To test whether the iEL/0-SCF approach reproduces all properties of any system when compared to the default PCG-SCF method used in TINKER, we have examined four very different physical systems: (1) homogeneous bulk water, (2) heterogeneous salt solutions, at three different concentrations of $MgCl_2$ in water: 0.30 M, 1.21 M, and 4.66 M, (3) a small solute, a zwitterionic glycine peptide in water, and (4) a larger protein, DHFR, in water. As we show in what follows, the iEL/0-SCF method can reproduce all of aspects of polarization compared to the standard SCF approach, and thus all energetic, structural, and dynamical properties of these four very different cases.

NVE and NVT conservation properties. Figure 1a shows the results when optimizing for the one free parameter γ that is needed to estimate the $\boldsymbol{\mu}_{SCF,i}$ solution using Eq. (14), examined by running the iEL/0-SCF method in the NVE ensemble with a range of γ values from 0 to 1. From this analysis we determine that the maximum stable value of γ is 0.92, with values greater than that yielding unstable trajectories, and values of $\gamma < 0.5$ yielding poor energy conservation. The best value of $\gamma = 0.9$ gives energy drifts that are commensurate with the standard PCG-SCF method. Figure 1b reports the 'pseudo-temperature' of the auxiliary dipoles in these simulations, defined as $T_{aux} = 1/3\langle \dot{\boldsymbol{a}}_i^2 \rangle$ since these dipoles do not have a mass, in which we see increases in inertia throughout the simulation, regardless of γ value. The rate of buildup of the auxiliary inertia degrades the real dipole dynamics through resonances as we have shown previously[28], therefore in the NVE ensemble we are restricted to time steps ~0.5 fs to realize good energy conservation for the real degrees of freedom.

Figure 1*: Energy conservation in the NVE and NVT ensembles for water.* (a) Energy along trajectories of the iEL/0-SCF method for a range of γ values. (b) The auxiliary pseudo-temperature, $T_{aux} = 1/3\langle \dot{\mathbf{a}}_i^2 \rangle$, of the simulations from (a). In (a) and (b) all NVE simulations used a time step of 0.5 fs. (c) Conserved energy of the extended system in the NVT ensemble (blue), along with the energy for the real degrees of freedom in the NVT ensemble of 512 water molecules using the iEL/0-SCF approach (red) and standard SCF approach (black). For the NVT simulations we used a time step of 1.0 fs, γ was set to 0.9, while the SCF solution used a PCG-SCF method with a convergence threshold of 10^{-6} RMS Debye.

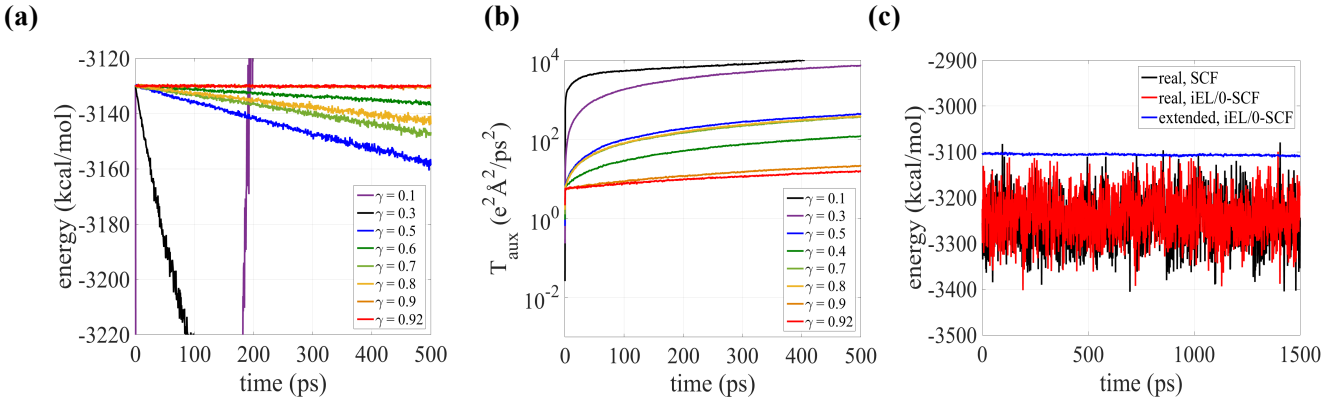

For the NVT ensemble simulations we require a thermostat applied to both real and auxiliary degrees of freedom, and thus we have a new conservation law that depends directly on an extended system that requires the auxiliary dipoles to be kept at a low effective temperature relative to the real degrees of freedom[42]. Figure 1c shows that this extended system quantity is well conserved (i.e. including all the thermostat variables) for water, when fitted using a fictitious mass of the auxiliary dipoles of 0.0103 g/mol/e^2 and which corresponds to a real temperature of 0.0656 K for the auxiliary dipoles, and allows for an increased time step of 1.0 fs. The NVT energies and fluctuations for the real nuclear degrees of freedom of water for the iEL/0-SCF method is in accord with the standard SCF benchmark over 3 ns

(Table 1 and Figure S1), and additional tests run out to tens of nanoseconds show that SCF and iEL/0-SCF solutions remained in quantitative agreement for all systems.

Table 1: *Ensemble average total energy and polarization energies for bulk water, salt solutions, and glycine dipeptide in water.* Average total potential energy, $\langle U \rangle$, and average polarization potential energy, $\langle U_{pol} \rangle$, for both a standard SCF method and the iEL/0-SCF approach. Data is generated from 3.0 ns trajectories in the NVT ensemble at 298.0 K; further simulation details are given in the text and SI material.

Bulk Water	**Method**	$\langle U \rangle$ **(kcal/mol)**	$\langle U_{pol} \rangle$ **(kcal/mol)**
	iEL/0-SCF	-4610+/-40	-2590+/-50
	SCF	-4620+/-40	-2570+/-50
Glycine in Water	iEL/0-SCF	-2420+/30	-1290+/-40
	SCF	-2430+/-30	-1300+/-30
0.3M $MgCl_2$	iEL/0-SCF	-8830+/-50	-4010+/-60
	SCF	-8850+/-50	-4040+/-70
1.21M $MgCl_2$	iEL/0-SCF	-15690+/-50	-5100+/-70
	SCF	-15710+/-50	-5070+/-70
4.66M $MgCl_2$	iEL/0-SCF	-43220+/-50	-9640+/-100
	SCF	-43220+/-50	-9490+/-90

Polarization properties. For bulk water we find that the average molecular dipole moment for a condensed phase water molecule yields a value of 2.81 Debye with both the PCG-SCF and iEL/0-SCF methods. The corresponding probability density distribution of real induced dipoles generated from the iEL/0-SCF solutions is in excellent agreement with the standard SCF solutions, regardless of system, as shown in Figure 2 and Figure S2.

Figure 2: *Comparison of induced dipole probability density distributions using the iEL/0-SCF and standard PCG-SCF methods.* (a) Hydrogen in bulk water, (b) the glycine carbonyl oxygen, and (c) Mg^{2+} for all $MgCl_2$ salt concentration for a standard SCF method (dashed) and our iEL/0-SCF method (solid). For plots (a) and (b) we consider the *x*, *y*, and *z* dipole components. For plot (c) we consider three different $MgCl_2$ salt concentrations of 0.30 M (black), 1.21 M (red), and 4.66 M (blue). The induced dipole distributions for water and glycine use an internal coordinate frame; see [43] for details on the internal coordinates.

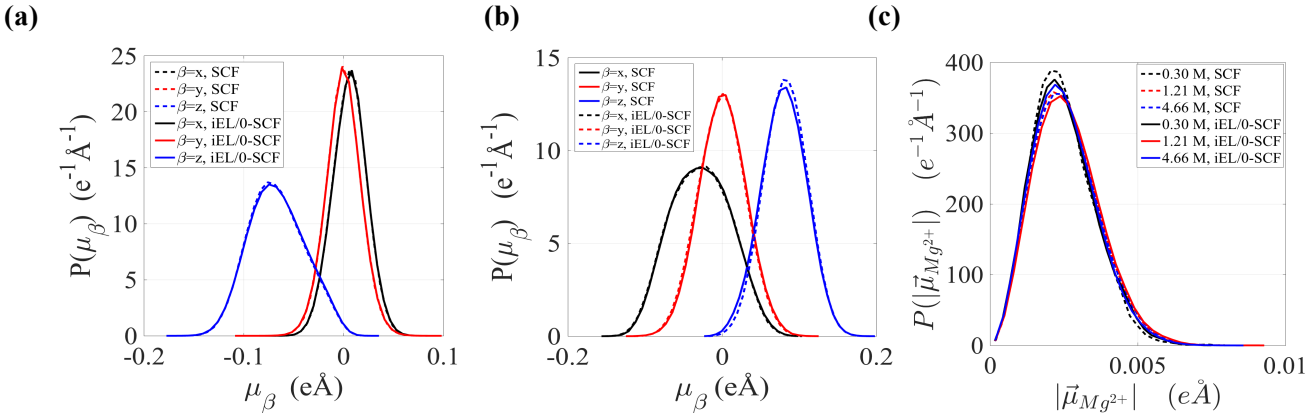

Dynamical properties. Using the NVE ensemble simulation, we calculate the self-diffusion constant of water to be 1.90 +/- 0.13 using the iEL/0-SCF approach and 2.02 +/- 0.20 for the standard SCF procedure. We also report the Mg^{2+} and Cl^{-} ion diffusion constants for the 4.66M concentration in Table S1 that show the two methods are in quantitative agreement. A particularly stringent time-dependent property in the NVT ensemble, the autocorrelation function for induced dipoles, demonstrates that the iEL/0-SCF method does not suffer from any loss of accuracy, regardless of system (Figure 3 and Figure S3). We can see that for both hydrogen and oxygen atoms for bulk water, Mg^{2+} and Cl^{-} for the salt solution (shown for 1.21M), and the backbone carbonyl carbon, carbonyl oxygen, nitrogen, and α-carbon of glycine dipeptide, that the iEL/0-SCF method reproduces the autocorrelations well, especially at the critical short time scale range less than about 0.2 ps over which there can be rapid changes in dipole direction (especially for bulk water).

Figure 3: *Comparison of dynamic polarization properties using the iEL/0-SCF and standard PCG-SCF methods.* Autocorrelation function of real dipole for (a) bulk water, (b) solvated glycine, and (c) Mg^{2+} and Cl^{-} for 1.21M salt concentrations with a standard SCF method (dashed) and our iEL/0-SCF method (solid). The induced dipole distributions for water and glycine used an internal coordinate frame; see [43] for details on the internal coordinates. All data is based on 30 ps trajectories in the NVT ensemble at 298.0 K.

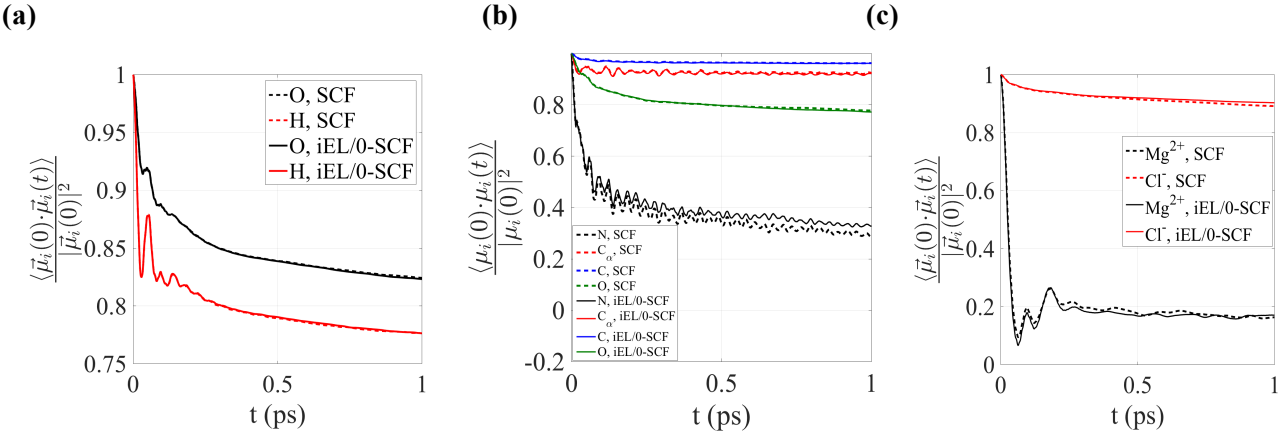

Structural properties. The iEL/0-SCF method also reproduces structural properties for all systems, in which Figure 4 and Figure S4 present the radial distribution functions for atom correlations of bulk water, the water oxygen and hydrogen correlations with the anion and cation of the salt solutions, and finally the water oxygen and hydrogen radial distribution functions with the glycine peptide backbone atoms. In summary, we see excellent agreement between the iEL/0-SCF method and the standard SCF solver.

Figure 4: *Comparison of radial distribution functions using the iEL/0-SCF and standard PCG-SCF methods* for (a) oxygen-hydrogen for bulk water, (b) water oxygen-backbone nitrogen and water hydrogen-backbone nitrogen of glycine dipeptide, and (c) water oxygen-Mg^{2+} and water hydrogen- Mg^{2+} for the 0.30 M salt concentrations for a standard SCF method (dashed) and our iEL/0-SCF method (solid). The induced dipole distributions for water and glycine used an internal coordinate frame; see [43] for details on the internal coordinates. All data is based on 3.0 ns trajectories in the NVT ensemble at 298.0 K.

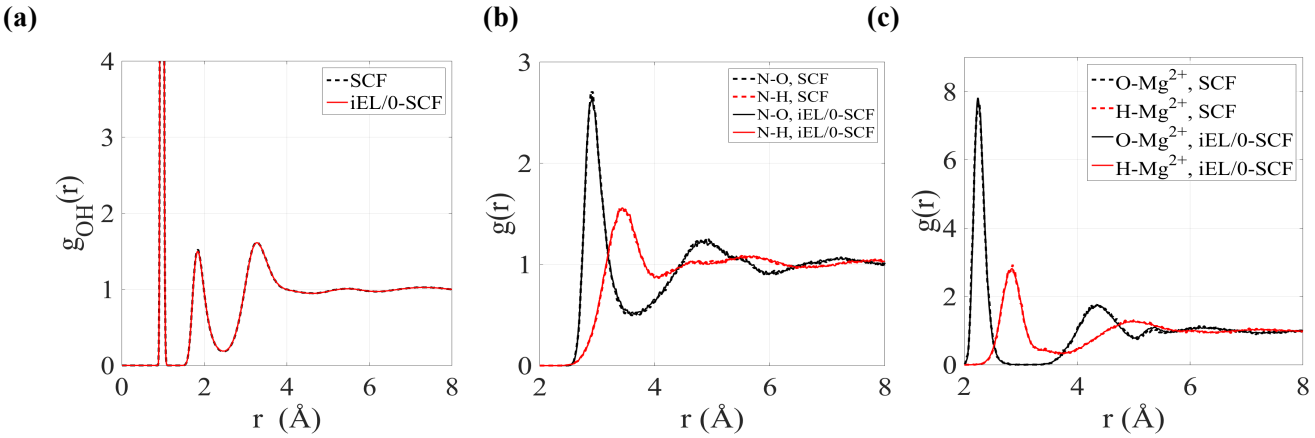

Timing Comparisons between iEL/0-SCF and PCG-SCF with and without multi-time stepping. The iEL/0-SCF method was implemented in the TINKER software package and takes advantage of the shared-memory parallelism of that code. While we have shown that the iEL/0-SCF method can reproduce the property results for any of the above systems when compared to the standard default convergence criteria used for the PCG-SCF solver in the TINKER code, we now examine the computational efficiency of the iEL/0-SCF method in the same code and on the same hardware platform using the default TINKER settings. Figure 5a shows the OpenMP scaling results in units of ns/day of the SCF and iEL/0-SCF methods applied to bulk water in which both use the same Verlet integration scheme with a time step of 1.0 fs. For 8 cores we see that the iEL/0-SCF method is 40% faster than the standard SCF solution, and since the iEL/0-SCF method also scales better to larger numbers of cores it rises to ~70% faster than the default polarization solution. In fact, when compared to a multi-time step RESPA[30] that uses a 2.0 fs outer time step, the iEL/0-SCF method is slightly faster at 16 cores, although it uses Verlet integration with a 1.0 fs timestep. Figure 5b shows the OpenMP scaling results as system size grows while holding the number of cores constant at 16 cores, for the standard SCF polarization result using either a RESPA[30] integration scheme with a 2.0 fs outer timestep, the Verlet integration with a 1.0 fs timestep, and the iEL/0-SCF approach that uses the Verlet integration scheme with a time step of 1.0 fs. Again, it is seen that the iEL/0-SCF approach is as fast as the RESPA scheme in timings for ns/day.

Figure 5: *Timing comparisons between iEL/0-SCF and standard iteration methods.* Simulation speed-up in nanoseconds per day for (a) OpenMP scaling as a function of the number of cores for a box of 512 water molecules in the NVT ensemble at 298.0 K and (b) OpenMP scaling for increasing system size with the number of cores fixed at 16. The methods that are compared include the iEL/0-SCF method at a time step of 1.0 fs (red), a preconditioned conjugate gradient solver integrated with Verlet at a time step of 1.0 fs (blue), and with a RESPA method using an outer time step of 2.0 fs (black). The real dipoles of the standard SCF methods in (b) were converged to 10^{-5} RMS Debye (solid), the standard default in TINKER.

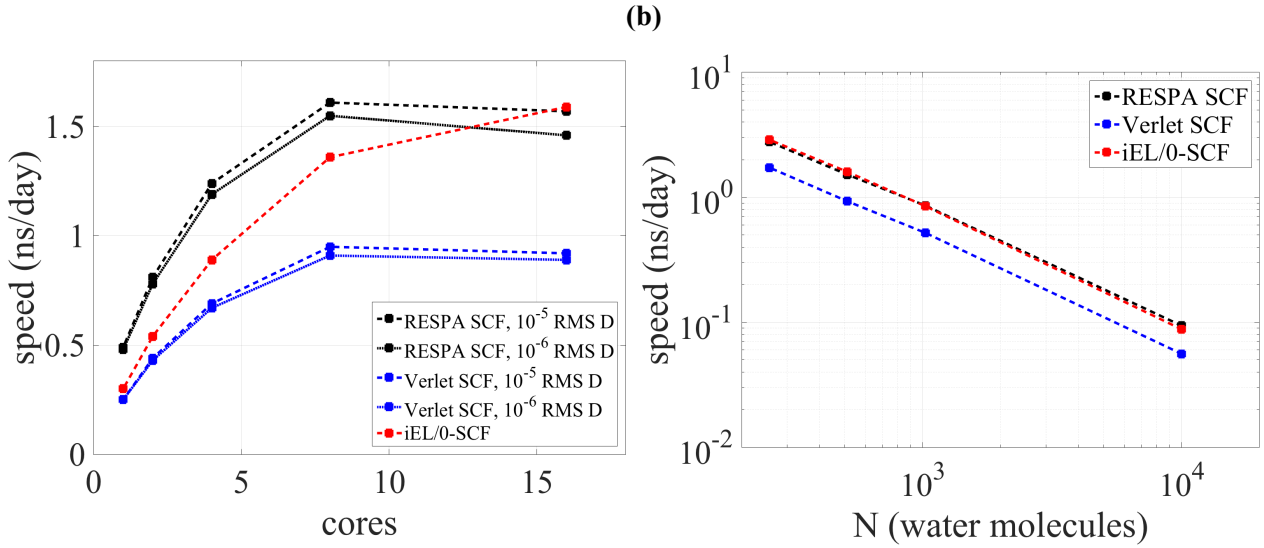

DISCUSSION

In general, energies, dynamical properties, and polarizability and structural correlations, are quantitatively produced by our iEL/0-SCF method when compared to the standard SCF solver for a diverse set of simple systems ranging from bulk water, dilute to concentrated salt solutions, and a small peptide in water. We also provide an additional stress test for our new iEL/0-SCF solution to the polarization equations by simulating a much larger biomolecular system, namely DHFR in water, the so-called Joint Amber-CHARMM benchmark. Table 2 gives the average potential energy and average polarization energy for the aqueous DHFR system when we use a single γ value for both the protein and the water solvent when defining the local kernel approximation for $\boldsymbol{\mu}_{SCF,i}$ in Eq. (9). For γ values greater than 0.7 we find that the aqueous DHFR simulations became unstable (which also happened for the other water-based systems when $\gamma > 0.92$), and ultimately $\gamma = 0.7$ was the best value that we found from numerical testing. In this case the differences between the iEL/0-SCF and SCF energy values are on the order of 1.0%, although this small difference is nonetheless outside numerical error bars.

Table 2: *Average total potential energy,* $\langle U \rangle$*, and polarization energy,* $\langle U_{pol} \rangle$*, for the iEL/0-SCF method for a protein in water using different values of* γ_S *and* γ_P *for the local kernel definition for solvent and protein.* Data is generated from 300 ps trajectories in the NVT ensemble at 298.0 K; further simulation details are given in the text and SI material.

Local Kernel	$\langle U \rangle$ **(kcal/mol)**	$\langle U_{pol} \rangle$ **(kcal/mol)**
$\gamma_s = \gamma_P = 0.7$	-66060+/-170	-31160+/-150
$\gamma_s = 0.9;\ \gamma_P = 0.1$	-66310+/-180	-31440+/-160
SCF	-66670+/-160	-31850+/-150

While this suggests that the iEL/0-SCF method is sensitive to the local kernel definition for γ, we found that we can use the same γ value for water of 0.9 (now referred to as γ_s with 's' for solvent) that we determined for all previous aqueous systems considered, and allow the protein to independently optimize to a new value of $\gamma_P = 0.1$ (Table 2). It is clear that basic properties of the protein system are reproduced with either a single or dual value of γ since the protein remains stable as measured by its root mean square deviation (RMSD) (Figure 6).

Figure 6: *Root mean square deviation calculated for the DHFR protein in water using the iEL/0-SCF and standard SCF method.* A single value of $\gamma = 0.7$ and dual values of $\gamma_S = 0.9$ and $\gamma_P = 0.1$ were used for the local kernel definition for solvent and protein. The PCG-SCF method (black) uses a Verlet with a 1.0 fs time step and 10^{-6} RMS Debye convergence, and the PCG-SCF method with RESPA (dashed gray) is PCG with a 2.0 fs outer time step and 10^{-5} RMS Debye convergence.

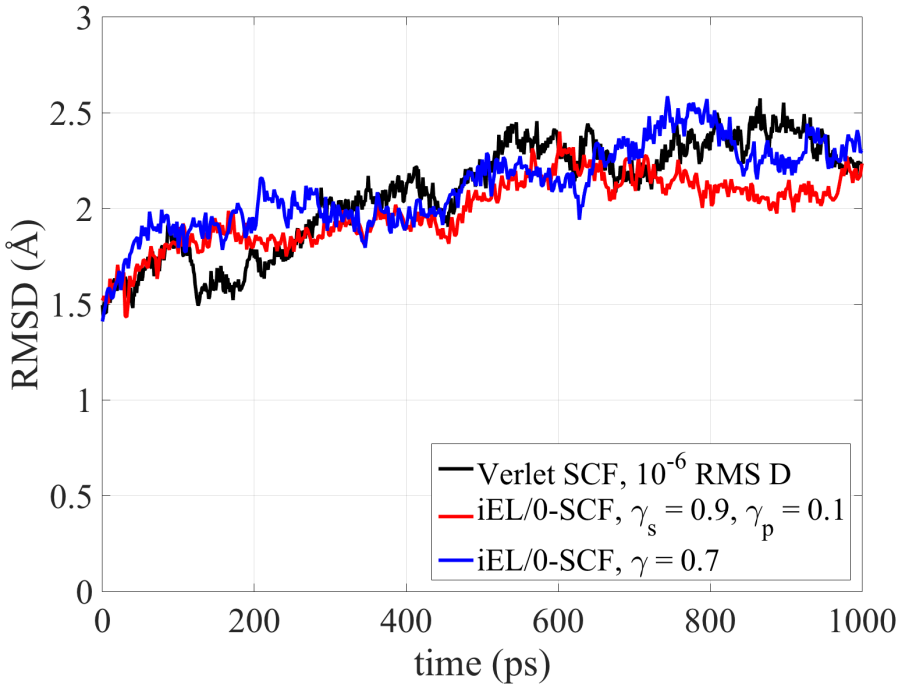

CONCLUSIONS

We have developed a new solution to classical polarization for molecular dynamics simulations that does not require any SCF iteration. The iEL/0-SCF method we have laid out here builds upon our iEL/SCF scheme[28], in that it continues to use an auxiliary set of induced dipoles that are dynamically integrated in a time-reversible manner, and which again serve as an initial guess for the real induced dipoles, but for the iEL/0-SCF method no further SCF cycles are required. Across all relevant systems typically studied in molecular simulation: a homogeneous fluid, ionic solutions, and small and large solutes in aqueous media, all ensemble averages over polarization properties are in good agreement between the SCF and iEL/0-SCF methods, and therefore by extension all physical properties of any system examined here are reproduced accurately. The iEL/0-SCF approach also realizes significant computational speedups when compared to an SCF method that uses a single 1.0 fs time step Verlet integration, and is as fast as that obtained by using RESPA with a 2.0 fs outer time step.

The iEL/0-SCF method is numerically stable over long simulation times, and we offer a qualitative explanation as to why the iEL/0-SCF scheme works as well as it does. First is that the form of the polarization energy and forces ensures that any deviations, δ, from the SCF solution only give rise to errors on the order of $O(\delta^2)$ in energy and forces. Second we suggest that, since the autocorrelation function for the real dipoles decay on a 100 fs timescale (using water as an example in Figure S3), then the repeated application of real dipole and auxiliary dipole updates every 1.0 fs, is effectively doing SCF iterations on the fly. In the end the iEL/0-SCF method achieves a correct full mutual polarization solution at the cost of direct polarization – a cost that is commensurate with the chosen level of permanent electrostatics.

We have recently applied both the dissipative dXL and iEL/SCF methods to the solution of the density in a linear scaling DFT implementation in the ONETEP software package, in which we showed that both methods are significant performance enhancements over standard SCF solutions for *ab initio* molecular dynamics[29]. One of the interesting outcomes in comparing the dissipative XL-BOMD and iEL/SCF approaches when applied to classical electric dipoles versus the quantum electron density is that while both schemes perform equally well in the latter, only the iEL/SCF method works in the case of classical polarization. More specifically, the small amount of broken time reversibility is negligible compared to the error in the linear scaling DFT forces, whereas classical polarization forces are close to exact so that the undesirable dissipative forces that destroy time reversibility are much in evidence. One lesson that is learned is that the classical polarization model provides a more stringent test for new many-body electronic solutions that may inform the *ab initio* molecular dynamics, and hence we are optimistic

that our iEL/0-SCF integration technique could also be applied to AIMD as an alternative to the modified Verlet integration of the equations of motion for the electronic degrees of freedom in the dissipative XL-BOMD method or for linear scaling DFT in ONETEP.

Other goals for future work include combining the iEL/0-SCF approach with RESPA[30] and /or isokinetic[44-45] methods to extend the integration time step further, and to examine the benefits in the use of non-local kernels for estimating the converged SCF solution. While the local kernel definition has proven reliable across a large diversity of systems, and the values of γ are easy to obtain through short NVE simulations, it does motivate a generalization of Eq. (14) to a 'non-local' kernel[27] to improve the iEL/0-SCF method in future work, provided such methods do not add significantly to the computational cost.

ACKNOWLEDGMENTS

AA and THG thank the National Science Foundation Grant No. CHE-1363320 for support of this work. A.M.N.N. acknowledges support from the Department of Energy Offices of Basic Energy Sciences (Grant No. LANL2014E8AN).

Supporting Information Available: Diffusion constants for pure water and 4.66 M $MgCl_2$ solution, nanosecond time scale energy trajectories for, additional induced dipole probability distributions, induced dipole autocorrelations, and radial distribution functions for all systems (water, $MgCl_2$ solutions, and solvated glycine) for both the iEL/0-SCF and standard SCF methods.

REFERENCES

1. Demerdash, O.; Yap, E. H.; Head-Gordon, T. Advanced potential energy surfaces for condensed phase simulation. *Annu Rev Phys Chem* **2014,** *65*, 149-174.
2. Stone, A. J. *The Theory of Intermolecular Forces*. Clarendon Press: Oxford,UK, 1996.
3. Shi, Y.; Ren, P.; Schnieders, M.; Piquemal, J. P. Polarizable Force Fields for Biomolecular Modeling. *Rev. Comp. Chem.* **2015,** *28*, 51-86.
4. Albaugh, A.; Boateng, H. A.; Bradshaw, R. T.; Demerdash, O.; Dziedzic, J.; Mao, Y.; Margul, D. T.; Swails, J.; Zeng, Q.; Case, D. A.; Eastman, P.; Essex, J. W.; Head-Gordon, M.; Pande, V. S.; Ponder, J. W.; Shao, Y.; Skylaris, C.-K.; Todorov, I. T.; Tuckerman, M. E.; Head-Gordon, T. Advanced Potential Energy Surfaces for Molecular Simulation. *J Phys Chem B (Feature article)* **2016,** *in press*.
5. Gresh, N.; Cisneros, G. A.; Darden, T. A.; Piquemal, J. P. Anisotropic, polarizable molecular mechanics studies of inter- and intramoecular interactions and ligand-macromolecule complexes. A bottom-up strategy. *Journal of Chemical Theory and Computation* **2007,** *3* (6), 1960-1986.
6. Jungwirth, P.; Winter, B. Ions at aqueous interfaces: From water surface to hydrated proteins. In *Annual Review of Physical Chemistry*, 2008; Vol. 59, pp 343-366.
7. Vazdar, M.; Pluharova, E.; Mason, P. E.; Vacha, R.; Jungwirth, P. Ions at Hydrophobic Aqueous Interfaces: Molecular Dynamics with Effective Polarization. *Journal of Physical Chemistry Letters* **2012,** *3* (15), 2087-2091.

8. Bhowmick, A.; Sharma, S.; Head-Gordon, T. Computational Improvements of a Designed Kemp Eliminase without Laboratory Directed Evolution. *J Am Chem Soc* **2017,** *in press*.
9. Fried, S. D.; Wang, L. P.; Boxer, S. G.; Ren, P.; Pande, V. S. Calculations of the electric fields in liquid solutions. *J Phys Chem B* **2013,** *117* (50), 16236-48.
10. Johnson, M.; Malardier-Jugroot, C.; Murarka, R.; Head-Gordon, T. Hydration water dynamics near biological interfaces. *Journal of physical chemistry B* **2009,** *113*, 4082-4092.
11. Johnson, M. E.; Malardier-Jugroot, C.; Head-Gordon, T. Effects of co-solvents on peptide hydration water structure and dynamics. *Physical Chemistry Chemical Physics* **2010,** *12*, 393-405.
12. Wang, L. P.; Head-Gordon, T.; Ponder, J. W.; Ren, P.; Chodera, J. D.; Eastman, P. K.; Martinez, T. J.; Pande, V. S. Systematic improvement of a classical molecular model of water. *J Phys Chem B* **2013,** *117* (34), 9956-72.
13. Wang, W.; Skeel, R. D. Fast evaluation of polarizable forces. *J Chem Phys* **2005,** *123*, 164107.
14. Lipparini, F.; Lagardère, L.; Stamm, B.; Cancès, É.; Schnieders, M.; Ren, P.; Maday, Y.; Piquemal, J.-P. Scalable Evaluation of Polarization Energy and Associated Forces in Polarizable Molecular Dynamics: I. Toward Massively Parallel Direct Space Computations. *J. Chem. Theory Comput.* **2014,** *10* (4), 1638-1651.
15. Lamoureux, G.; Roux, B. Modeling induced polarization with classical Drude oscillators: Theory and molecular dynamics simulation algorithm. *J Chem Phys* **2003,** *119* (6), 3025-3039.
16. Belle, D. V.; Froeyen, M.; G.Lippens; Wodak, S. J. Molecular dynamics simulation of polarizable water by an extended Lagrangian method. *Molecular Physics* **1992,** *77* (2), 239-255.
17. Császár, P.; Pulay, P. Geometry optimization by direct inversion in the iterative subspace. *Journal of Molecular Structure* **1984,** *114*, 31-34.
18. Lagardère, L.; Lipparini, F.; Polack, É.; Stamm, B.; Cancès, É.; Schnieders, M.; Ren, P.; Maday, Y.; Piquemal, J.-P. Scalable Evaluation of Polarization Energy and Associated Forces in Polarizable Molecular Dynamics: II. Toward Massively Parallel Computations Using Smooth Particle Mesh Ewald. *J. Chem. Theory Comput.* **2015,** *11* (6), 2589-2599.
19. Simmonett, A. C.; Pickard, F. C.; Shao, Y.; Cheatham, T. E., III; Brooks, B. R. Efficient treatment of induced dipoles. *J Chem Phys* **2015,** *143* (7).
20. Simmonett, A. C.; Pickard, F. C. t.; Schaefer, H. F., 3rd; Brooks, B. R. An efficient algorithm for multipole energies and derivatives based on spherical harmonics and extensions to particle mesh Ewald. *J Chem Phys* **2014,** *140* (18), 184101.
21. Simmonett, A. C.; IV, F. C. P.; Ponder, J. W.; Brooks, B. R. An empirical extrapolation scheme for efficient treatment of induced dipoles. *The Journal of Chemical Physics* **2016,** *145* (16), 164101.
22. Aviat, F.; Levitt, A.; Stamm, B.; Maday, Y.; Ren, P.; Ponder, J. W.; Lagardère, L.; Piquemal, J.-P. Truncated Conjugate Gradient: An Optimal Strategy for the Analytical Evaluation of the Many-Body Polarization Energy and Forces in Molecular Simulations. *Journal of Chemical Theory and Computation* **2017,** *13* (1), 180-190.
23. Niklasson, A. M.; Tymczak, C. J.; Challacombe, M. Time-reversible Born-Oppenheimer molecular dynamics. *Phys Rev Lett* **2006,** *97* (12), 123001.
24. Niklasson, A. M.; Tymczak, C. J.; Challacombe, M. Time-reversible ab initio molecular dynamics. *J Chem Phys* **2007,** *126* (14), 144103.
25. Niklasson, A. M. Extended Born-Oppenheimer molecular dynamics. *Phys Rev Lett* **2008,** *100* (12), 123004.
26. Niklasson, A. M.; Steneteg, P.; Odell, A.; Bock, N.; Challacombe, M.; Tymczak, C.; Holmström, E.; Zheng, G.; Weber, V. Extended Lagrangian Born–Oppenheimer molecular dynamics with dissipation. *The Journal of chemical physics* **2009,** *130* (21), 214109.
27. Niklasson, A. M.; Cawkwell, M. J. Generalized extended Lagrangian Born-Oppenheimer molecular dynamics. *J Chem Phys* **2014,** *141* (16), 164123.

28. Albaugh, A.; Demerdash, O.; Head-Gordon, T. An efficient and stable hybrid extended Lagrangian/self-consistent field scheme for solving classical mutual induction. *J Chem Phys* **2015,** *143* (17), 174104.
29. Vitale, V.; Dziedzic, J.; Albaugh, A.; Niklasson, A. M. N.; Head-Gordon, T.; Skylaris, C.-K. Performance of extended Lagrangian schemes for molecular dynamics simulations with classical polarizable force fields and density functional theory. *J. Chem. Phys.* **2017,** *submitted*.
30. Tuckerman, M.; Berne, B. J.; Martyna, G. J. Reversible multiple time scale molecular dynamics. *The Journal of chemical physics* **1992,** *97* (3), 1990-2001.
31. Demerdash, O. N.; Head-Gordon, T. Convergence of the Many-Body Expansion for Energy and Forces for Classical Polarizable Models in the Condensed Phase. *J. Chem. Theory Comput.* **2016,** *in press*.
32. Car, R.; Parrinello, M. Unified Approach for Molecular-Dynamics and Density-Functional Theory. *Physical Review Letters* **1985,** *55* (22), 2471-2474.
33. Lamoureux, G.; MacKerell, A. D.; Roux, B. A simple polarizable model of water based on classical Drude oscillators. *J Chem Phys* **2003,** *119* (10), 5185-5197.
34. Kolafa, J. Time-reversible always stable predictor–corrector method for molecular dynamics of polarizable molecules. *Journal of Computational Chemistry* **2004,** *25* (3), 335-342.
35. Ponder, J. W. *TINKER: Software Tools for Molecular Design, Version 7.0*, http://dasher.wustl.edu/tinker/, Washington University in St. Louis, June 2014.
36. Laury, M. L.; Wang, L. P.; Pande, V. S.; Head-Gordon, T.; Ponder, J. W. Revised Parameters for the AMOEBA Polarizable Atomic Multipole Water Model. *J Phys Chem B* **2015**.
37. Wang, L. P. Simtk.org: ForceBalance: Systematic Force Field Optimization. https://simtk.org/home/forcebalance (accessed Feb. 23, 2013).
38. Ren, P. Y.; Wu, C. J.; Ponder, J. W. Polarizable Atomic Multipole-Based Molecular Mechanics for Organic Molecules. *Journal of Chemical Theory and Computation* **2011,** *7* (10), 3143-3161.
39. Esser, A.; Belsare, S.; Marx, D.; Head-Gordon, T. Mode specific THz spectra of solvated amino acids using the AMOEBA polarizable force field. *Physical chemistry chemical physics : PCCP* **2017,** *19* (7), 5579-5590.
40. Swope, W. C.; Andersen, H. C.; Berens, P. H.; Wilson, K. R. A computer simulation method for the calculation of equilibrium constants for the formation of physical clusters of molecules: Application to small water clusters. *The Journal of Chemical Physics* **1982,** *76*, 637.
41. Martyna, G. J.; Klein, M. L.; Tuckerman, M. Nosé–Hoover chains: the canonical ensemble via continuous dynamics. *The Journal of chemical physics* **1992,** *97* (4), 2635-2643.
42. Blochl, P. E.; Parrinello, M. ADIABATICITY IN 1ST-PRINCIPLES MOLECULAR-DYNAMICS. *Physical Review B* **1992,** *45* (16), 9413-9416.
43. Ren, P.; Ponder, J. W. Consistent treatment of inter- and intramolecular polarization in molecular mechanics calculations. *J Comput Chem* **2002,** *23* (16), 1497-506.
44. Leimkuhler, B.; Margul, D. T.; Tuckerman, M. E. Stochastic, resonance-free multiple time-step algorithm for molecular dynamics with very large time steps. *Molecular Physics* **2013,** *111* (22-23), 3579-3594.
45. Margul, D. T.; Tuckerman, M. E. A Stochastic, Resonance-Free Multiple Time-Step Algorithm for Polarizable Models That Permits Very Large Time Steps. *Journal of Chemical Theory and Computation* **2016,** *12* (5), 2170-2180.

Appendix A: AMOEBA Force Field p- and d-Scaling

The AMOEBA force field uses scaling to exclude certain electrostatics based on bond separation, as these terms are modeled implicitly in bonded valence terms like bonds, angles, bond-angle, torsion, etc. The forms of the electrostatic interactions are scaled differently depending on their form and type. Permanent-permanent interactions are scaled by a factor known as 'm-scaling' and induced-induced interactions are scaled by 'u-scaling', both of which are determined by the number of bonds separating the species to be scaled. Permanent-induced interactions, however, are scaled differently depending on whether the calculation is determining the induced dipoles or calculating the polarization energy. The former calculation relies on the polarization group the species are in and is referred to as 'd-scaling' while the latter relies on bond separation and is referred to as 'p-scaling'. For small species like water and ions there is no difference between p-scaling and d-scaling because the entire molecule is a single polarization group. When this is the case the equations presented in the body of the text are sufficient, but when larger molecules with multiple polarization groups are considered we need to adapt our equations accordingly.

For a general case with distinct p- and d-scaling we can start with a general definition of the polarization energy in Eq. (A1).

$$U^{pol}(\boldsymbol{r^N}) = \frac{1}{2}\boldsymbol{\mu}^d\boldsymbol{C}\boldsymbol{\mu}^p - \frac{1}{2}\boldsymbol{\mu}^d\boldsymbol{E}^p - \frac{1}{2}\boldsymbol{\mu}^p\boldsymbol{E}^d \tag{A1}$$

Here, again, $\boldsymbol{\mu}$ refer to a vector of all of the individual induced dipoles, $\boldsymbol{\mu}_i$, and $\boldsymbol{C}$ is a super-matrix made up of individual matrices $\boldsymbol{C}_{ij} = (\alpha_j^{-1}\delta_{ij} - \boldsymbol{T}'_{ij})$ where $\boldsymbol{T}'_{ij}$ is the dipole-dipole interaction tensor between sites i and j and α_i is the polarizability of site i. $\boldsymbol{E}$ represents a vector of all of electric fields at each site, $\boldsymbol{E}_i$, and the superscripts p and d refer to whether this electric field was calculated with the p-scaled or d-scaled permanent-induced interaction tensor $\boldsymbol{T}$, $\boldsymbol{E}^p = \boldsymbol{T}^p\boldsymbol{M}$ or $\boldsymbol{E}^d = \boldsymbol{T}^d\boldsymbol{M}$, respectively. The two sets of induced dipoles, then, correspond to dipoles calculated with the p- or d-scaled permanent fields, $\boldsymbol{\mu}^p = \alpha(\boldsymbol{E}^p + \boldsymbol{T}'\boldsymbol{a}^p)$ or $\boldsymbol{\mu}^d = \alpha(\boldsymbol{E}^d + \boldsymbol{T}'\boldsymbol{a}^d)$, respectively. It should be noted that in the completely converged SCF limit $\boldsymbol{\mu}^d = \boldsymbol{C}^{-1}\boldsymbol{E}^d$ and $\boldsymbol{\mu}^p = \boldsymbol{C}^{-1}\boldsymbol{E}^p$ and Eq. (A1) reduces to the familiar $U^{pol} = -\frac{1}{2}\boldsymbol{\mu}^d\boldsymbol{E}^p$. In practice, then, Eq. (A1) is used in place of Eq. (7).

We also need to evaluate the potential gradient so that we can determine forces. Including both the geometric term and dipole response terms yields Eq. (A2).

$$\left.\frac{dU^{pol}(\boldsymbol{r^N},\boldsymbol{a^N})}{d\boldsymbol{r}}\right|_{\boldsymbol{a}} = \frac{\partial U^{pol}(\boldsymbol{r^N},\boldsymbol{a^N})}{\partial \boldsymbol{r}} + \frac{\partial U^{pol}(\boldsymbol{r^N},\boldsymbol{a^N})}{\partial \boldsymbol{\mu}^p}\frac{\partial \boldsymbol{\mu}^p}{\partial \boldsymbol{r}} + \frac{\partial U^{pol}(\boldsymbol{r^N},\boldsymbol{a^N})}{\partial \boldsymbol{\mu}^d}\frac{\partial \boldsymbol{\mu}^d}{\partial \boldsymbol{r}} \tag{A2}$$

We can evaluate the full gradient since we know that we are evaluating the real dipoles using only a single electrostatic field calculation and the auxiliary dipoles as the initial guess, ie. $\boldsymbol{\mu}^p = \alpha(\boldsymbol{E}^p + \boldsymbol{T}'\boldsymbol{a}^p)$ and $\boldsymbol{\mu}^d = \alpha(\boldsymbol{E}^d + \boldsymbol{T}'\boldsymbol{a}^d)$. Substituting this into Eq. (A2) gives the polarization gradient for the real degrees of freedom, Eq. (A3).

$$\left.\frac{dU^{pol}(\boldsymbol{r}^N,\boldsymbol{a}^N)}{d\boldsymbol{r}}\right|_{\boldsymbol{a}} = -\frac{1}{2}[\,\boldsymbol{\mu}^d]^T\frac{\partial \boldsymbol{T}'}{\partial \boldsymbol{r}}\boldsymbol{\mu}^p + \frac{1}{2}[\,\boldsymbol{\mu}^d - \alpha\boldsymbol{T}\boldsymbol{\mu}^d - \alpha\boldsymbol{E}^d]^T\frac{\partial \boldsymbol{T}'}{\partial \boldsymbol{r}}\boldsymbol{a}^p - \frac{1}{2}[\alpha\boldsymbol{T}\boldsymbol{\mu}^d + \alpha\boldsymbol{E}^d]^T\frac{\partial \boldsymbol{T}^p\boldsymbol{M}}{\partial \boldsymbol{r}} + \frac{1}{2}[\,\boldsymbol{\mu}^p - \alpha\boldsymbol{T}\boldsymbol{\mu}^p - \alpha\boldsymbol{E}^p]^T\frac{\partial \boldsymbol{T}'}{\partial \boldsymbol{r}}\boldsymbol{a}^d - \frac{1}{2}[\alpha\boldsymbol{T}\boldsymbol{\mu}^p + \alpha\boldsymbol{E}^p]^T\frac{\partial \boldsymbol{T}^d\boldsymbol{M}}{\partial \boldsymbol{r}} \quad \text{(A3)}$$

Again, in the SCF limit, ie. $\boldsymbol{a} \rightarrow \boldsymbol{\mu} \rightarrow \boldsymbol{\mu}_{SCF}$, Eq. (A3) reduces to the familiar form from the AMOEBA potential and in the limit that p-scaling and d-scaling are identical we recover Eq. (19).